On the Ratio of Full-Resonance to Square-Root-Impedance Amplifications for Shear-Wave Velocity Profiles That Are a Continuous Function of Depth

David M. Boore*[1] and Norman A. Abrahamson[2]

ABSTRACT

Amplifications of seismic waves traveling upward through a continuous, interface-free velocity profile are consistently smaller when computed using the square-root-impedance (SRI) method than when computed using full-resonance (FR) calculations. This was found for a wide range of velocity profiles. For realistic profiles, for which the gradient of velocity decreases with depth, the differences are not large, with the ratio of FR/SRI amplifications ranging from about 1.05 to 1.3. Comparisons of the amplifications from a continuous velocity profile with those from approximations to that profile using a stack of constant-velocity layers give some support to the hypothesis that the difference between FR and SRI amplifications for gradient profiles is because the former is controlled by the ratio of seismic impedances, whereas the latter is based on the square root of the seismic impedance ratios. This implies that gradient profiles will always have FR amplifications greater than SRI amplifications. A model-independent, easy-to-implement modification of the SRI amplifications is proposed that shows promise in bringing the SRI amplifications closer to the FR amplifications.

KEY POINTS

- Are square-root-impedance amplifications always less than full-resonance amplifications for gradient models? Yes, but by at most a factor of 0.75 for realistic gradient models.
- Despite the consistent underestimation, square-root-impedance amplifications are useful in many applications.

INTRODUCTION

The square-root-impedance (SRI) method for computing site amplifications (e.g., Boore, 2013, hereafter B13) is widely used in simulations of ground-motion intensity measures (e.g., Boore, 2003), particularly for velocity profiles characterized by a smoothly varying depth dependence without significant step changes in seismic impedance. Such profiles are usually associated with generic site profiles used in deriving average amplifications from source depths to near the surface but not including any near-surface response. These amplifications are often termed "crustal" amplifications to distinguish them from "local" amplifications. The crustal amplifications are often used in stochastic simulations of ground motions (e.g., Boore, 2003). Profiles with step changes in impedance arise most commonly in site-specific applications, in which full-resonance (FR) amplifications show that these step changes can lead to strong resonance peaks. For convenience, "FR" and "SRI" are often used in the figures in this article as shorthand for "full-resonance amplification (A_{FR})" and "square-root-impedance amplification (A_{SRI})," respectively.

B13 discussed the comparison of A_{FR} and A_{SRI} for several profiles with constant-velocity layers and profiles in which the velocity is continuous with depth (in this article we sometimes use "gradient profiles" to describe continuous, interface-free velocity profiles). For the former, A_{SRI} underestimated A_{FR} at all resonance peaks, but A_{SRI} equals or is close to the root mean square (rms) of the total response (peaks and troughs) at frequencies higher than the fundamental mode frequency

1. U.S. Geological Survey, Earthquake Science Center, Moffett Field, California, U.S.A., https://orcid.org/0000-0002-8605-9673 (DMB); 2. Department of Civil and Environmental Engineering, University of California, Berkeley, California, U.S.A., https://orcid.org/0000-0001-7900-6023 (NAA)

*Corresponding author: dboore@yahoo.com

Cite this article as Boore, D. M., and N. A. Abrahamson (2023). On the Ratio of Full-Resonance to Square-Root-Impedance Amplifications for Shear-Wave Velocity Profiles That Are a Continuous Function of Depth, *Bull. Seismol. Soc. Am.* **113**, 1192–1207, doi: 10.1785/0120220197

(Day, 1996). For the gradient profiles, A_{SRI} was less than A_{FR} for almost all frequencies, the exception being for low frequencies in which A_{FR} is generally a few percent lower than A_{SRI}, although both amplifications for these frequencies are close to unity. Poggi *et al.* (2011) also found that A_{SRI} was less than A_{FR} for gradient profiles, as shown in their figure 13. In addition, F. Scherbaum drew attention to the difference in a 23 December 2010 technical note prepared for the Pegasos Refinement Project (P. Renault, personal comm., 2011). None of these people speculated on the reasons for the differences. A possible explanation of the reason for the differences is one purpose of this article. Another purpose is simply to document the persistent underestimation of A_{FR} by the SRI method for a number of gradient profiles (but for realistic profiles the underestimation is about a factor of 1.1, which is comparable to the epistemic uncertainty in ground-motion prediction models; Al Atik and Youngs, 2014).

This article starts with a brief review of the SRI method for computing amplifications. This is followed by a section comparing A_{FR} and A_{SRI} for several continuously varying profiles. After showing that A_{SRI} persistently underestimates A_{FR}, there is a section investigating a hypothesis as to why this is so. An unsuccessful attempt to relate the underestimation to characteristics of the velocity profile is discussed in the Relating A_{FR}/A_{SRI} to Velocity Profile Characteristics section, and the penultimate section contains a model-independent, easy-to-implement modification of A_{SRI} that shows promise in bringing A_{SRI} closer to A_{FR}.

BRIEF REVIEW OF SRI AMPLIFICATIONS

This is a brief summary of the detailed explanation of the method for SRI amplifications given by Boore (2003). Given a shear-wave velocity versus depth function $V(z)$, the amplification is given by

$$A(f(z)) = \left(\frac{Z_S}{\bar{Z}(f)}\right)^{\eta}, \tag{1}$$

in which $\eta = 0.5$. Z_S is the seismic impedance near the source, given by

$$Z_S = \rho_S V_S, \tag{2}$$

and ρ_S and V_S are the density and shear-wave velocity near the source. $\bar{Z}(f)$ is an average of seismic impedance from the surface to a depth z corresponding to a quarter wavelength for a wave with frequency f. The average seismic impedance is given by

$$\bar{Z}(f) = \bar{\rho}\,\bar{V}, \tag{3}$$

in which

$$\bar{\rho} = \frac{1}{z(f)}\int_0^{z(f)} \rho(z)dz, \tag{4}$$

and

$$\bar{V} = z(f)\left[\int_0^{z(f)} \frac{1}{V(z)}dz\right]^{-1}. \tag{5}$$

The depth z corresponds to a quarter wavelength for the frequency f and the time-averaged velocity $\bar{V}$ from the surface to z, as given implicitly in this equation:

$$f(z) = 1/\left[4\int_0^{z(f)} \frac{1}{V(z)}dz\right]. \tag{6}$$

In practice, it is easiest to specify the depth z and then compute f, $\bar{\rho}$, and $\bar{V}$ for that depth.

No damping is included in the amplifications; this is standard practice in the SRI method. The effect of damping is subsequently incorporated through the κ_0 operator $\exp(-\pi\kappa_0 f)$. Because the purpose in this article is to compare SRI amplifications with A_{FR}, the latter also do not include damping.

EXAMPLES OF THE RATIO OF A_{FR} AND A_{SRI}

This article includes ratios of A_{FR} and A_{SRI} for the following profiles (shown in Fig. 1):

- Profiles for which $V_{S30} = 760$ m/s (Fig. 1a):
  - The Al Atik and Abrahamson (2021) velocity profile from inversions of response spectra from the Chiou and Youngs (2014) ground-motion prediction model (hereafter, AAA21[CY14]). This profile was extended linearly from 6.05 km (the bottom of the profile in AAA21) to a depth of 8 km.
  - The BJ97gr760 profile of Boore (2016) (hereafter, B16), corresponding to a revision of the Boore and Joyner (1997) velocity profile for a generic rock site. The base of the profile is at 8 km.
  - An approximation of the Kamai *et al.* (2013) (hereafter, Kea13) profile. The Kea13 profile consists of a stack of constant-velocity layers (CVLs), but because this article is about profiles with continuously varying velocities with depth, we constructed a continuous approximation of the Kea13 profile. We did this by replacing each interface with a single velocity that was the average of the velocities above and below each interface, and then these average velocities were connected by straight lines. The travel time to the bottom of the profile is very close to the travel time for the CVL profile. The base of the profile is at 8 km.
- A suite of profiles, with $V_{S30} = 360$, 760, 1000, 1500, and 2000 m/s (Fig. 1c, which shows the profiles for $V_{S30} = 360$, 760, and 1500 m/s). The velocity models were derived from extrapolations (for $V_{S30} = 360$ m/s) or interpolations (for the other models) of the Boore and Joyner (1997) generic rock and generic hard-rock profiles using

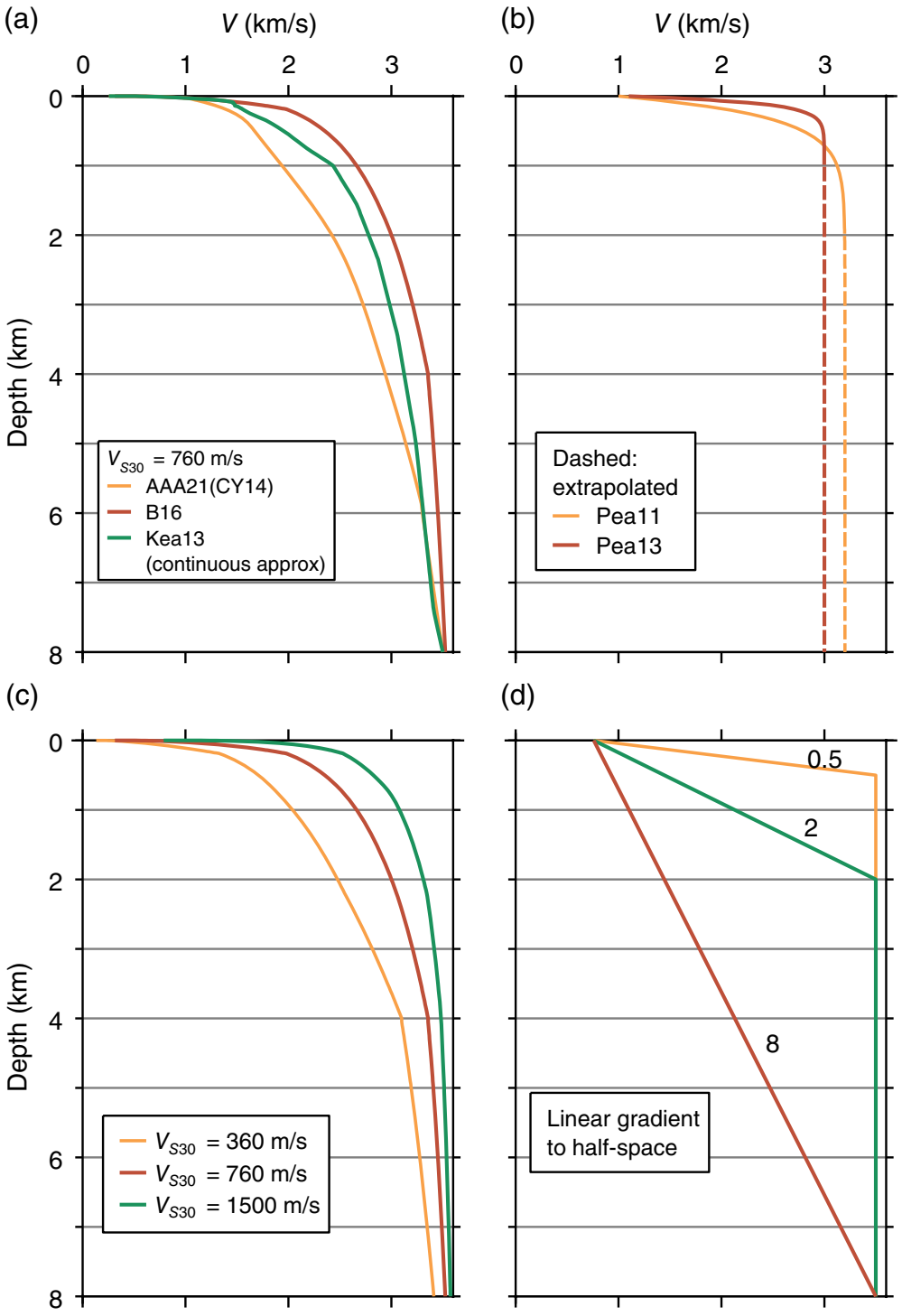

Figure 1. Shear-wave velocity versus depth for all models used in this article (see section Examples of the Ratio of A_{FR} and A_{SRI} for details). (a) Profiles for which V_{S30} = 760 m/s. (b) Gradient profiles from Poggi *et al.* (2011, 2013). (c) Profiles for which V_{S30} = 360, 760, and 1500 m/s. (d) A suite of profiles with a single linear gradient from the surface to a constant-velocity halfspace. The color version of this figure is available only in the electronic edition.

the interpolation method discussed in Boore (2016). The base of each profile is at 8 km.

- Gradient profiles from Poggi *et al.* (2011, 2013) (hereafter Pea11 and Pea13) (Fig. 1b). The Pea11 and Pea13 profiles had a base depth of 2 and 1 km and V_{S30} = 1. and 1 .34 km/s, respectively. The profiles were extended to 8 km by adding a CVL with the velocity of the base of the Pea11 and Pea13 profiles.
- A suite of profiles with a single linear gradient from the surface to a constant-velocity half-space (Fig. 1d). These profiles are included as an extreme example of profiles with a continuous variation of velocity with depth. The gradient of the previous profiles decreased with depth, whereas these profiles have a constant gradient.

A_{SRI} is computed using *site_amp_batch* (see the Data and Resources section), which can use a velocity profile made up of any sequence of CVLs or linear line segments connecting velocity-depth points. A_{FR}, on the other hand, is computed using *nrattle*, which requires a velocity profile that is a stack of CVLs, whereas this article is focused on velocity profiles without step changes in velocity (and the associated density). To resolve this apparent inconsistency, we replaced the continuous velocity profiles by profiles with many equivalent CVLs; each had a very small jump in the seismic impedance (the step changes are barely perceptible in plots of the velocity to 8 km), such that the travel time with depth was the same for both the gradient profiles and the CVL approximation of the gradient profiles. Typically, 1200 CVLs were used to represent the velocity from the surface to 8 km. Experiments with varying numbers of layers reassured us that the approximation of a gradient profile by an equivalent CVL profile with many layers gives an accurate representation of the amplifications for the

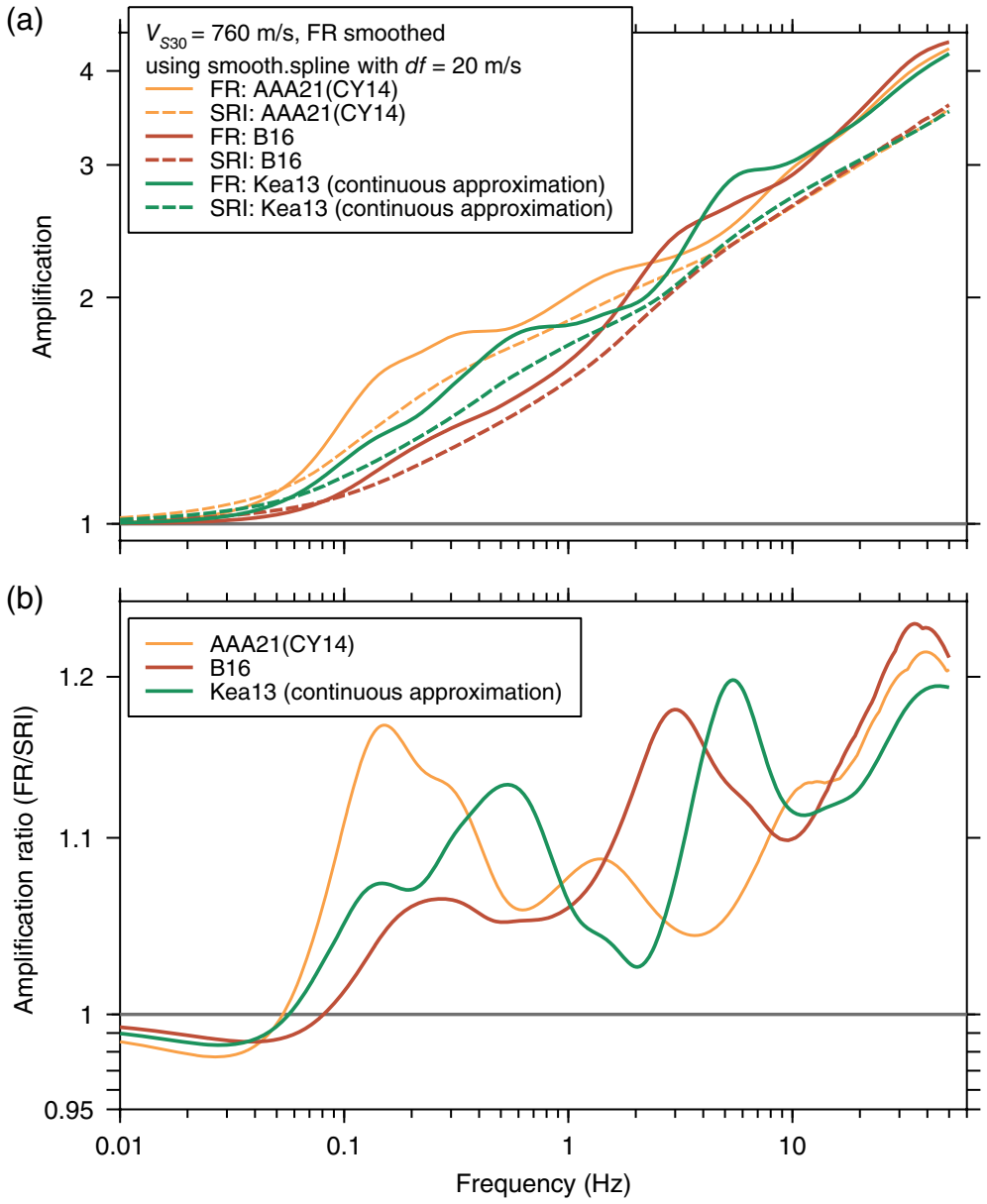

Figure 2. (a) Square-root-impedance (SRI) and full-resonant (FR) amplifications and (b) the ratio of the amplifications for three profiles with velocities that have V_{S30} = 760 m/s and are a continuous function of depth, with no discontinuities. The color version of this figure is available only in the electronic edition.

gradient profile. We use a multilayer representation of the continuous velocity profile to allow the computation of the amplification without restrictions about the profile. There are analytical solutions for specific continuous profiles, such as those described by Schreyer (1977); however, when using these solutions, we lose the generality afforded by our approach.

Each profile was placed over a half-space with a velocity and density close to that at the bottom of the models (to avoid a large impedance contrast at the base of the models). The seismic impedance for the bottom-most CVL in the models was often slightly different than the half-space density and velocity. Owing to the lack of attenuation in A_{FR} calculations, this produced some very small, but noticeable, rapid oscillations in A_{FR} when plotted against frequency. The oscillations are overtones of the fundamental-mode resonance from the surface to the base of the profile base above the added half-space. In the plots shown in this section, the small oscillations were removed from the amplifications by a spline-smoothing operator; the underlying trends were not affected by the smoothing.

A_{FR} and A_{SRI} and A_{FR}/A_{SRI} ratios for the AAA21(CY14), B16, and Kea13 profiles are shown in Figure 2. Although the amplifications differ in detail, A_{FR}/A_{SRI} ratios for all profiles are similar in increasing from near unity at low frequencies to a value near 1.2 at high frequencies. The ratio is greater than unity for all frequencies, with the exception of low frequencies corresponding to quarter-wavelength (QWL) depths that are in the half-space below the velocity profile, and in this case both A_{SRI} and A_{FR} are close to unity.

Although the form of the graphs in Figure 2 is traditional, with the frequency being plotted on the abscissa, it can be informative to plot the amplifications and A_{FR}/A_{SRI} ratios versus depth. Aside from being a compact display of the velocities and the amplifications, we hope that the plots might give insights into the relation of A_{FR}/A_{SRI} to characteristics of the velocity profiles. A plot of the amplifications versus depth can be done because there is a mapping in the SRI method between frequency and depth (equation 6). This is shown in Figure 3, in which the top graph corresponds to the traditional plot, with frequency on the abscissa, the middle plot shows the mapping of the QWL depth and frequency, and the bottom graph shows A_{FR}, A_{SRI}, and A_{FR}/A_{SRI} versus QWL depth.

Figures 4 and 5 show the velocity profile, A_{SRI}, A_{FR}/A_{SRI}, and the QWL frequency as a function of depth, for the various

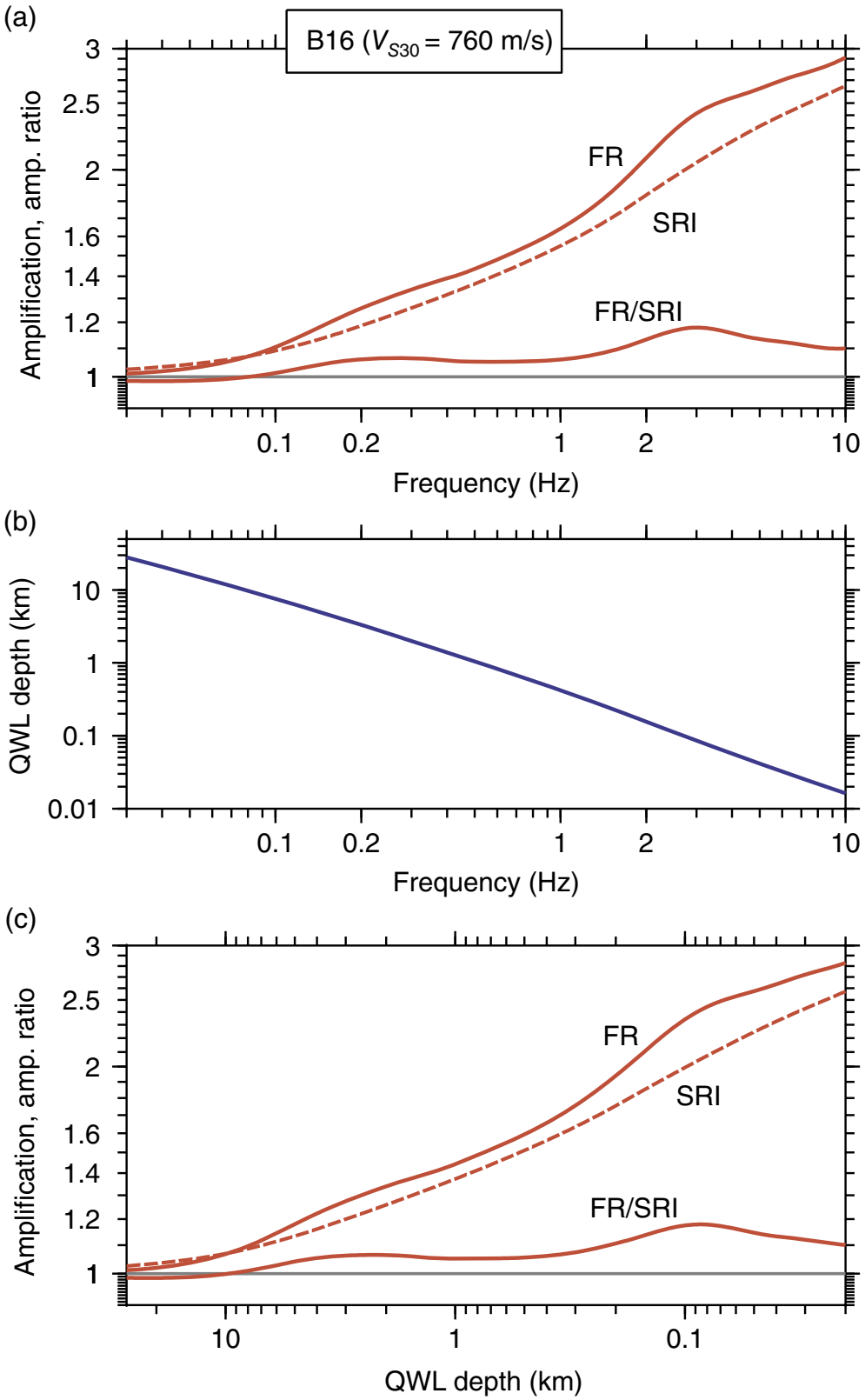

Figure 3. Illustration of how the amplifications and ratio of amplifications can be plotted as a function of the quarter-wavelength (QWL) depth for the velocity profile from Boore (2016) (B16). (a) The amplifications and ratio of amplifications plotted against frequency. (b) The mapping of frequency to QWL depth. (c) The amplifications and ratio of amplifications plotted against depth. The color version of this figure is available only in the electronic edition .

continuously varying profiles described at the beginning of this section. Figure 4 shows the results for the three profiles used in Figure 2. Although it is hard to see because of the depth range shown, the peak of A_{FR}/A_{SRI} corresponds to depths <100 m for the Kea13 and B16 profiles. The exception is the AAA21(CY14) profile, for which the depth corresponding to the maximum FR/SRI amplification ratio is 3.5 km. This feature is due to the Chiou and Youngs (2014) model having a large relative site response at low frequencies, as shown in Figure 2 of Al Atik and Abrahamson, (2021). The bottom graph in Figure 4 shows the results for profiles derived from interpolations or extrapolations of the Boore and Joyner (1997) generic rock (BJ97gr) and generic very hard-rock (BJ97gvhr) profiles using the interpolation method described by Boore (2016). The results are similar to those in the top graph of the figure, with A_{FR}/A_{SRI} being greater than unity except at very low frequencies.

A_{FR}/A_{SRI} for velocity profiles that are quite different than those used in Figure 4 are shown in Figure 5. As with the profiles in Figure 4, all of the A_{FR}/A_{SRI} ratios are >1.0 (and are close to 1.4 for the linear gradient profiles) except for frequencies that correspond to depths in the half-spaces added to the bases of the models. In addition, it is easy to see in Figure 5 that the peaks of A_{FR}/A_{SRI} occur at frequencies corresponding to about the midpoint of the gradient portion of the profiles; such a relation is not obvious for the profiles in Figure 4.

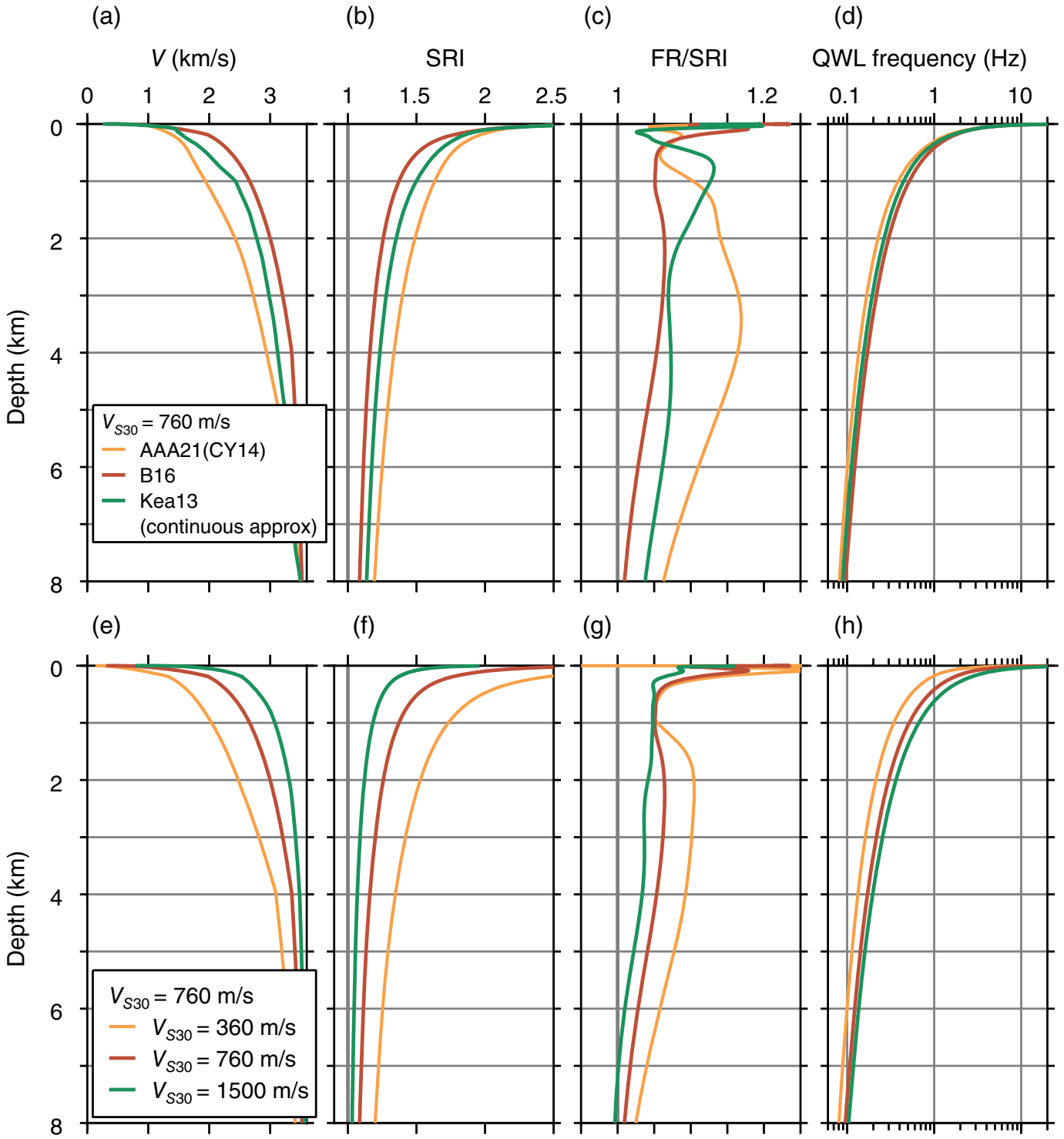

Figure 4. The graphs in the rows show (a,e) the velocity profiles, (b,f) SRI amplification, (c,g) ratio of FR to SRI amplifications, and (d,h) the quarter-wavelength frequencies as a function of depth for the models shown in the legend in the leftmost graph in each row. The color version of this figure is available only in the electronic edition.

SUGGESTED REASON FOR A_{SRI} TO UNDERESTIMATE A_{FR}

Based on the results in Figures 4 and 5, as well as the results of other studies (e.g., Douglas *et al.*, 2009; Poggi *et al.*, 2011; Boore, 2013), it seems to be well established that the amplifications computed using the SRI method underestimate A_{FR} for velocity profiles that are a continuous function of depth, with no step changes in seismic impedance. This underestimation is well known for velocity profiles with significant step changes in the seismic impedance, as shown in Figure 6. In the figure, the peaks of A_{FR} are given by the ratio of seismic impedances (density times velocity) for this simple one-layer

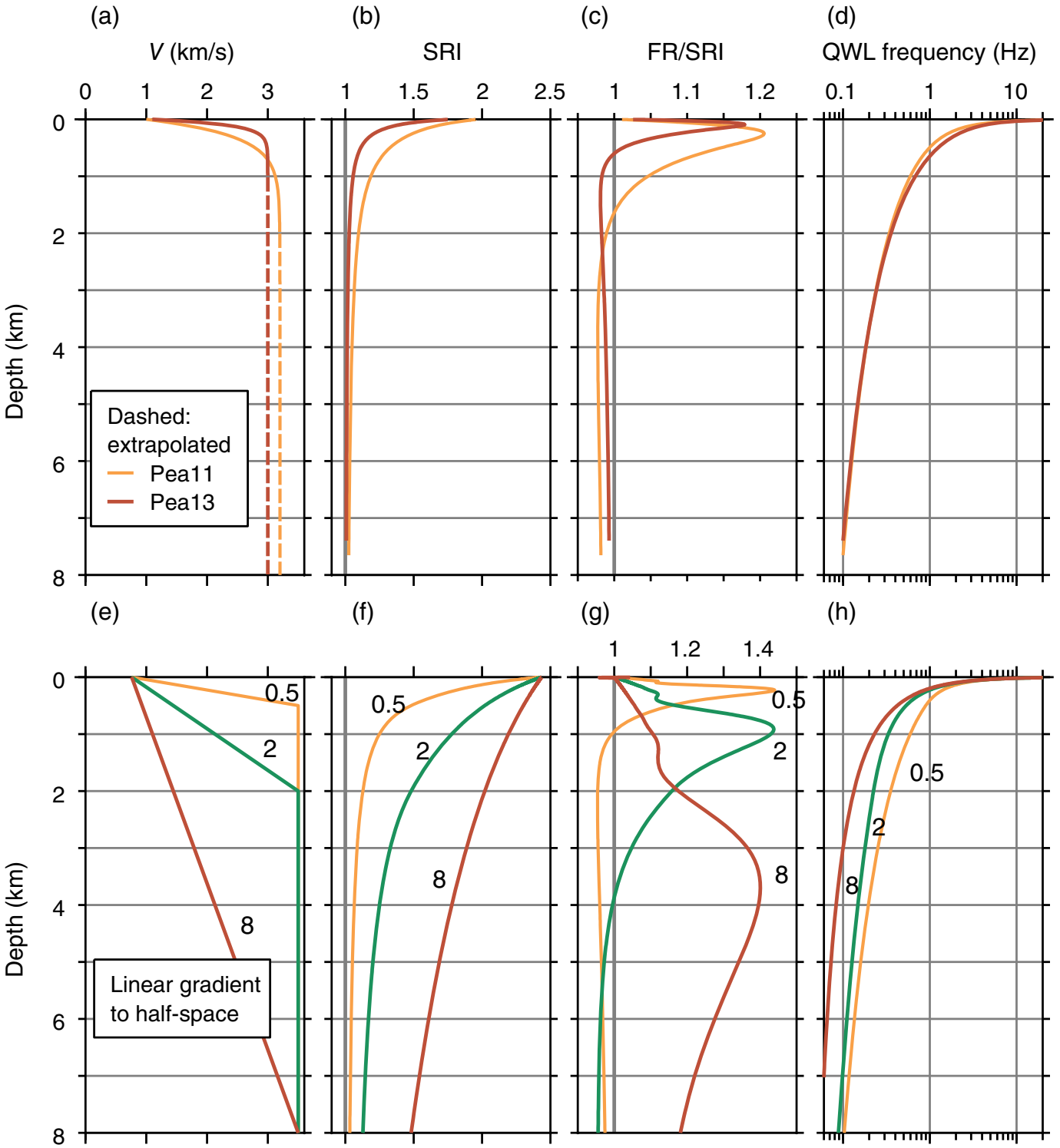

profile, whereas A_{SRI} is given by the square root of the ratio of seismic impedances. We think that this difference carries over to more complicated velocity profiles, in which A_{FR} can be thought of as being composed of the peak resonances for many layers. If correct, fundamentally the difference in A_{FR} and A_{SRI} is due to A_{FR} being related to the ratio of seismic impedances in the profile rather than to the square root of the seismic impedances, which is at the core of the SRI method. We have not, however, been able to find a way to verify

Figure 5. The graphs in the rows show (a,e) the velocity profiles, (b,f) SRI amplification, (c,g) ratio of FR to SRI amplifications, and (d,h) the quarter-wavelength frequencies as a function of depth for the models shown in the legend in the leftmost graph in each row. The numbers in the graphs in the lower row are depths, in kilometers, to the constant velocity layer at the base of each model. The color version of this figure is available only in the electronic edition.

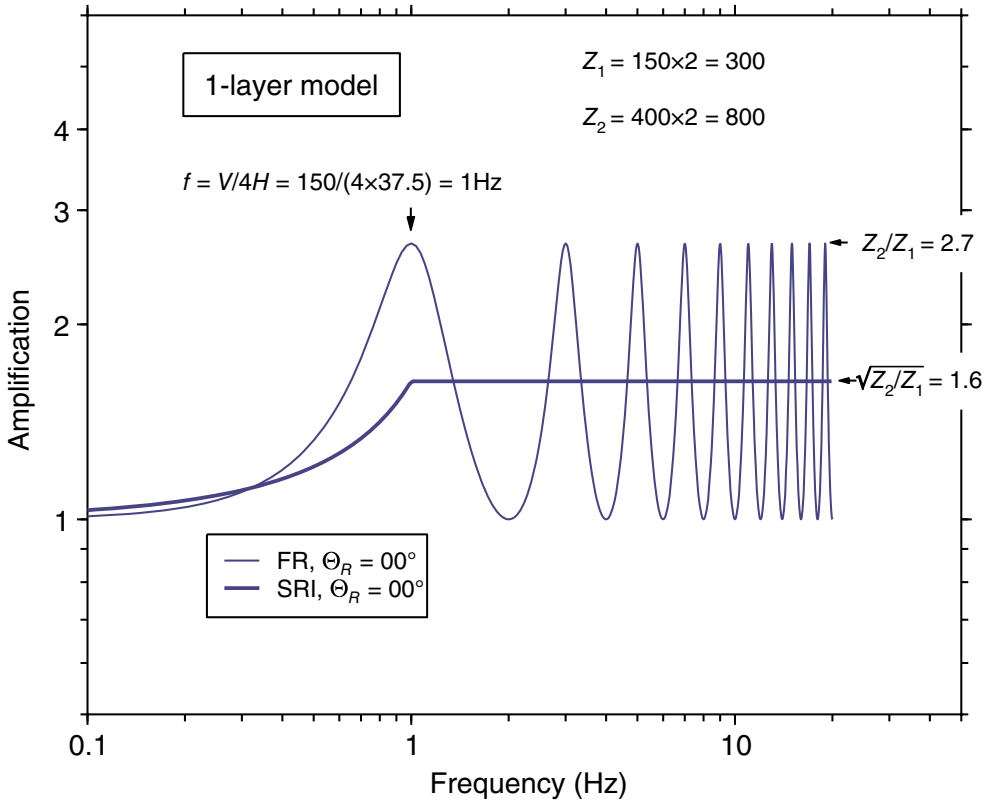

Figure 6. The amplification for a velocity profile with a constant-velocity layer (150 m/s) over a constant-velocity half-space (400 m/s). The density (2 gm/cc) is the same in the layer and the half-space. Z is the seismic impedance, and Θ_R is the angle of incidence. (Revised from Figure 4 in Boore, 2013). The color version of this figure is available only in the electronic edition.

this hypothesis theoretically or to use this insight to devise a procedure to adjust A_{SRI} for specific gradient profiles so that they are consistent with A_{FR}, short of replacing A_{SRI} with A_{FR}. Instead, we will illustrate the differences between A_{FR} and A_{SRI} for a suite of seven profiles composed of a stack of CVLs that divided the velocity from the surface to 8 km into 5–320 layers, with the number of layers increasing by a factor of two between each set. The CVL profiles are equivalent to a gradient profile. By "equivalent," we mean that the travel time from the surface to the bottom of any layer is the same as the travel time from the surface of the gradient profile to the same depth as the bottom of the layer (see the Data and Resources section for notes on obtaining equivalent velocity profiles). We chose the BJ97gr760 profile of B16 as the gradient profile for this exercise (this is the same as the profile labeled "B16" in Figs. 2–4). The gradient profile and the CVL approximations to the profile are shown in Figure 7.

A_{FR} and A_{SRI} are shown in Figure 8. The amplifications are relative to a half-space with V = 3.5 km/s and ρ = 2.72 gm/cc. Two aspects of the results shown in Figure 8 warrant discussion: the frequency of the first amplification maximum for each CVL profile and the amplitude of that maximum compared with A_{FR} and A_{SRI} for the gradient profile at that frequency. Some properties and results for the CVL profiles, of relevance for this discussion, are included in Table 1.

Frequency of peak amplifications for CVL profiles

The lowest frequency of the peak A_{FR} for each CVL profile corresponds to the QWL frequency for the shallowest layer in each profile. These frequencies are shown by vertical lines in Figure 8. For example, the shallowest layer in the 20-layer profile has a thickness of 0.167 km and a velocity of 1.275 km/s, giving a QWL frequency of $f_{0.25\lambda} = V/(4H) =$ 1.91 Hz. Below this frequency, Figure 8 shows that the FR response of each CVL profile follows the trend of the gradient-profile A_{FR} (and as expected, becomes closer to that amplification as the numbers of layers increase in the CVL profiles). Above the frequency of the A_{FR} peak amplification, the CVL response resembles the response of a single-layer constant-velocity profile, with a series of peaks and troughs.

Amplifications of CVL profiles

As shown in Figure 8, A_{FR} for the CVL profiles at the lowest peak frequency for each CVL model are always somewhat above the gradient-model A_{FR} at that frequency, with the CVL amplitudes approaching the gradient-profile amplitudes for frequencies less than the lowest peak frequency as the number of layers increases, as expected. In addition, comparing A_{FR} to A_{SRI}, Figure 8 shows that $A_{FR} > A_{SRI}$ for all frequencies less than a frequency somewhat greater than the resonant frequency corresponding to the shallowest layer of the CVL model (except for very low frequencies, as noted in the discussion of Fig. 2); for convenience, the ratio of A_{FR} to A_{SRI} for the gradient profile is included in Figure 8.

To obtain some insight into what might be controlling the size of A_{FR}, in Table 1 we compare the observed amplifications to those for simple models. Columns 7 and 8 of the table contain amplifications based on ratios of the seismic impedances ($Z = \rho V$, in which ρ and V are density and velocity, respectively) using two extremes for the reference impedance in the numerator: the impedance of the second layer in the

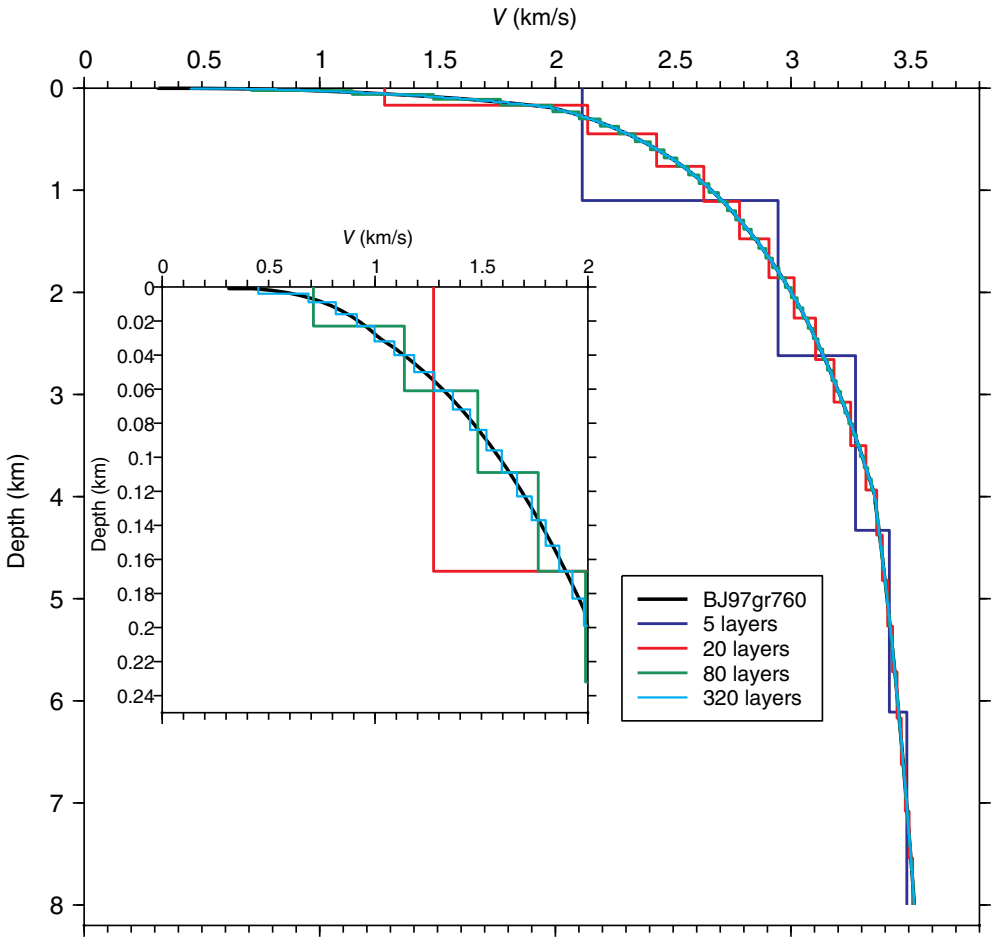

Figure 7. The continuous BJ97gr760 profile from Boore (2016) and its approximation by profiles with 5, 20, 80, and 320 constant-velocity layers. Profiles with 10 and 160 CVLs were also used but are not shown to avoid clutter. The color version of this figure is available only in the electronic edition.

CVL profile and the impedance of the half-space. The amplifications are given by the ratio of the impedances and as such are the peak amplifications for a layer over a half-space, an assumption with decreasing validity as the number of layers increases. Despite this caveat, the CVL-profile and gradient-profile amplifications (columns 9 and 10 in Table 1) are between the predictions based on the ratio of seismic impedances (columns 7 and 8 in Table 1) and are always above the SRI amplifications for the gradient profile.

Both the frequencies and the amplitudes of the CVL amplifications are consistent with the FR response for a gradient profile being built up of the fundamental mode resonance responses of many layers.

RELATING A_{FR}/A_{SRI} TO VELOCITY PROFILE CHARACTERISTICS

It would be useful if the A_{FR}/A_{SRI} ratio could be related to characteristics of velocity profiles that are a continuous function of depth. If so, it would be possible to take advantage of the simplicity of the SRI method for computing amplifications and yet compute an adjustment factor for each velocity profile that would make the amplifications equivalent to the amplifications from the FR method. As shown in Figure 6, a profile with a single constant-velocity layer over a half-space (with an infinite slope in velocity versus depth at the interface depth) leads to a pronounced resonance peak for which amplitude is given by the ratio of seismic impedances below and above the interface. Based on this, we hypothesized that the size of A_{FR}/A_{SRI} for gradient profiles would be a function of the gradient of the velocity profile with depth, with the ratio decreasing as the gradient decreased. The results for the linear profiles, shown in the bottom row of graphs in Figure 5, are not consistent with this hypothesis, as A_{FR}/A_{SRI} for all the profiles have the same maximum.

To look for a correlation of the maximum A_{FR}/A_{SRI} ratio with the gradient of the profile, we selected the maximum of A_{FR}/A_{SRI} for each velocity profile considered in this article and tabulated the depth corresponding to the frequency of the maximum and the velocity gradient at that depth. We show the results in Figure 9. Except for very shallow depths, the linear profiles have an essentially constant maximum A_{FR}/A_{SRI} ratio. That constant maximum (1.44) is greater than the ratio for the more realistic profiles, for which the gradient of velocity decreases with depth; the maximum of A_{FR}/A_{SRI} for the realistic profiles ranges from 1.05 to 1.26. For most of the profiles, the depth associated with the maximum of A_{FR}/A_{SRI} is quite shallow (<100 m). There is no apparent correlation of the maximum of A_{FR}/A_{SRI} with the gradient of velocity, except for the shallowest linear gradient profile. We looked for a correlation of the maximum A_{FR}/A_{SRI} ratio with the curvature of the velocity as a function of depth, with similar negative results.

A MODIFICATION TO THE SRI AMPLIFICATION

In the SRI model, the amplification scales with the square root of the impedance ratio (equation (1) with $\eta = 0.5$), whereas in the FR model, the amplification for a one-layer profile scales with the impedance ratio (equation 1 with $\eta = 1.0$), as shown in Figure 6.

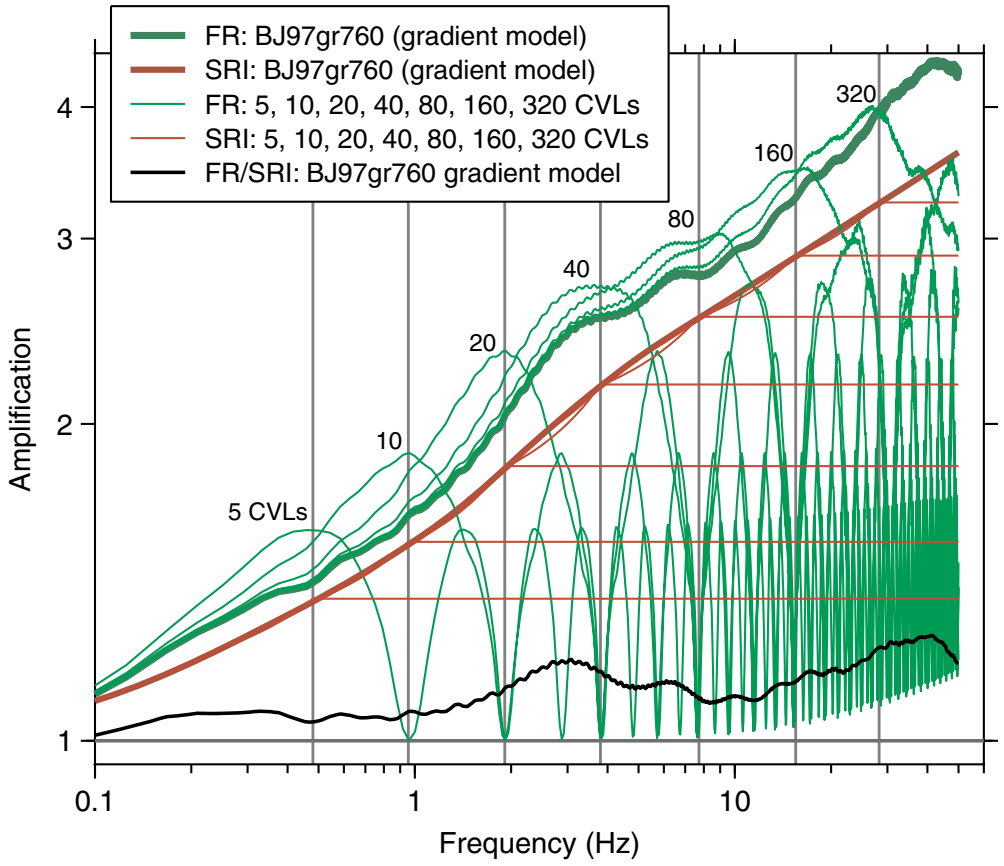

Figure 8. Amplifications for the various profiles. The number of layers in the CVL profiles is given by a number above the curve for that profile; the vertical line to the right of the number is the resonant frequency for the uppermost layer in the CVL profile. The low-amplitude, rapid oscillations are overtones caused by a very small impedance change at ~8 km, in which the density and velocity at the bottom of the profiles do not match exactly the half-space values of 2.72 gm/cc and 3.5 km/s, respectively. The oscillations have been smoothed out in the previous figures but have been retained here to show the overtones of the various CVL profiles. (These overtones are smoothed out when a spline smoothing operator is used that removes the small, rapid oscillations.) No attempt has been made to distinguish the CVL amplifications for frequencies much above that of the fundamental modes because these parts of the amplifications are not important for the discussion in this article. The color version of this figure is available only in the electronic edition.

For multiple layers, A_{FR} will not scale as strongly as for a one-layer profile. These considerations suggest a modification to the amplifications computed by the SRI method using equation (1) with the exponent η between 0.5 and 1.0. To investigate this possibility, we computed η for each of the velocity models considered in the article using this equation:

$$\eta = \frac{1}{2}\frac{\log(A_{FR})}{\log(A_{SRI})}. \qquad (7)$$

We used smoothed A_{FR} to reduce the low-amplitude, rapid oscillations caused by small impedance mismatches. The results are shown in Figure 10a. Although there is some similarity in shapes, the curves of η versus f are spread over a range of frequencies. Plotting η against the normalized frequency f/f_{bot}, in which f_{bot} is the QWL frequency corresponding to the bottom of each velocity model, tends to bring together the curves for each model (Fig. 10b), suggesting a common dependence of η on normalized frequency. Although the argument above suggests that η should be between 0.5 and 1.0, the results in Figure 10 show some values <0.5. These

TABLE 1
Properties of Selected Constant-Velocity Layer (CVL) Profiles

Model*	Layer	Thick (km)	V (km/s)	ρ (gm/cc)	$f_{0.25\lambda}$† (Hz)	$A = Z_2/Z_1$‡	$A = Z_{ref}/Z_1$§	A_{FR}: CVL‖	A_{FR}: Gradient‖
20 CVLs	1	0.167	1.275	2.24	1.91	1.81	3.33	2.34	2.03
	2	0.280	2.137	2.42					
	18 more	:	:	:					
80 CVLs	1	0.023	0.711	2.10	7.72	1.68	6.38	2.97	2.76
	2	0.038	1.138	2.21					
	78 more	:	:	:					

*All profiles are underlain by a 3.5 km/s and 2.72 gm/cc half-space.
†Quarter-wavelength frequency for first layer.
‡Z_1 and Z_2 are the impedances (ρV) in layers 1 and 2, respectively.
§$Z_{ref} = 2.72 \times 3.5$ (half-space density and velocity).
‖A_{FR} is the full-resonance (FR) amplitude at the quarter-wavelength frequency for the CVL and gradient profiles.

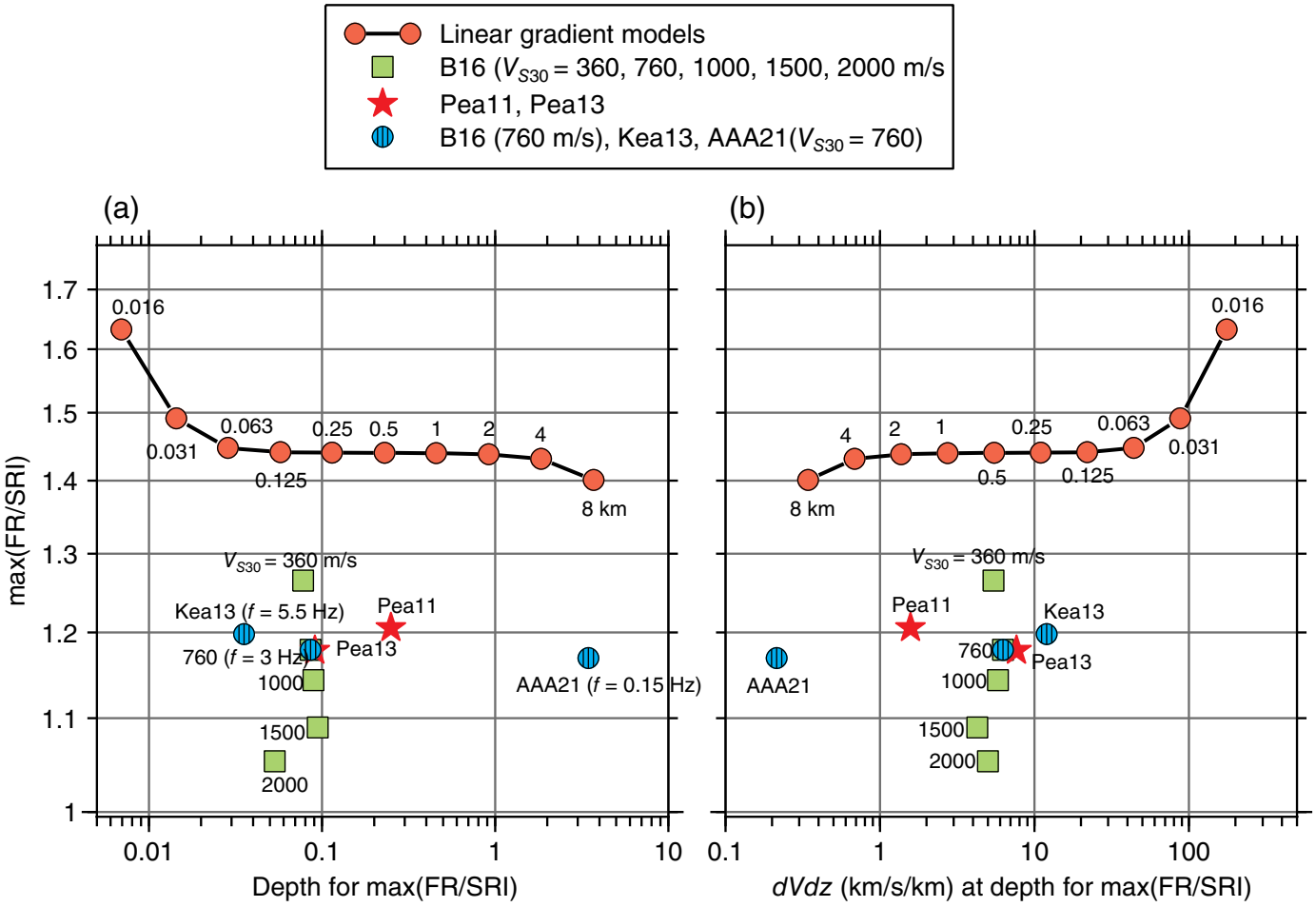

Figure 9. (a) Dependence of the maximum FR/SRI amplification ratio on the depth corresponding to the frequency at which the maximum occurred (shown in parentheses for three of the profiles). (b) Dependence of the maximum FR/SRI amplification ratio on the gradient of velocity at the depth corresponding to the frequency at which the maximum occurred. Note that for all but the linear gradient profiles, only frequencies <10 Hz are considered in finding the maximum FR/SRI amplification ratio; higher frequencies, associated with very shallow depths, are of little importance to ground-motion simulations, particularly after a damping operator is applied. The linear gradient profiles only had a single peak. Also note that the FR/SRI ratios for the B16 profile include values for V_{S30} = 1000 and 2000 m/s not shown in Figure 4, and the linear gradient profiles includes many more depths-to-profile-bottom than shown in Figure 5. The color version of this figure is available only in the electronic edition.

correspond to low frequencies in which A_{FR}/A_{SRI} can be <1.0 (as shown, for example, in Fig. 2). These low frequencies correspond to the average impedance ratios being determined by averages of velocities that extend into the half-spaces below the velocity profiles, with corresponding amplifications near unity. We have chosen not to constrain η to be between 0.5 and 1.0 because doing so would have negligible consequences on the amplifications.

To find an η function to be used in computing the modified SRI amplifications, we computed the mean of five velocity models that extended to depths of 8 km (the other model extending to 8 km was the linear model, which is not realistic). The models and the mean are shown in Figure 10c. The shape of η versus f/f_{bot} reminded us of the response of a harmonic oscillator to displacement. We chose the harmonic oscillator response as the functional form to fit the mean η and adjusted the coefficients in that function until a good fit was found between the mean-η curve and the function. The final function is shown in Figure 10c. The equation is

$$\eta = \frac{a(\frac{x-b}{s})^d}{\{[1-(\frac{x-b}{s})^e]^g + h(\frac{x-b}{s})^p\}^q}, \tag{8}$$

in which

$$x = \log\frac{f}{f_{bot}}. \tag{9}$$

and the logarithm is base 10. The coefficients are given in Table 2. The misfit in Figure 10c for small values of f/f_{bot} is not important because as mentioned earlier in this section, those frequencies correspond to extrapolations into the assumed uniform half-space.

We used equation (1) with the η function given by equation (8) to compute amplifications for all of the velocity

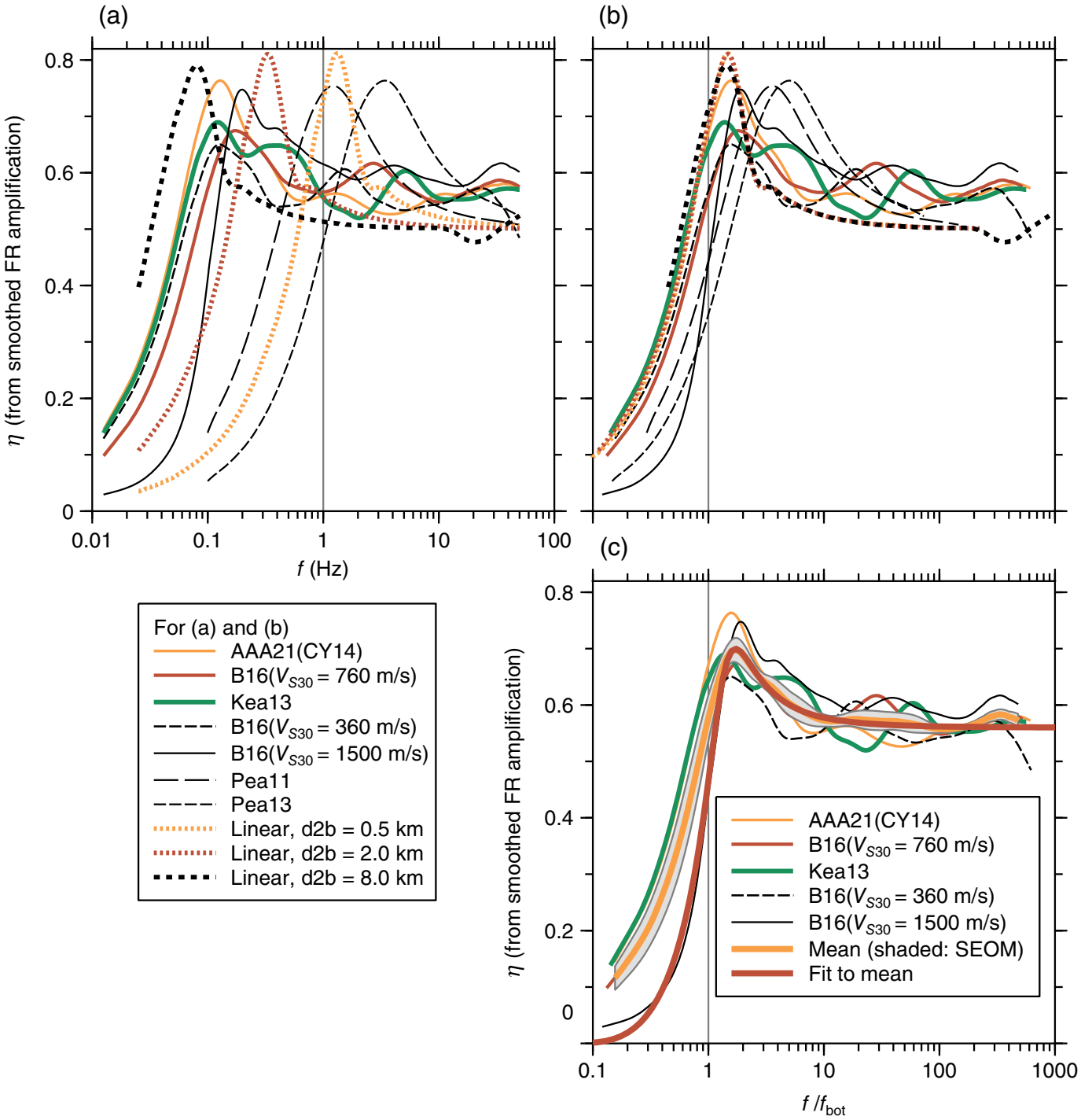

Figure 10. (a) The exponent η computed from equation (7) for all the velocity models considered in this article, plotted as a function of frequency. (b) The same as graph (a), except plotted as a function of frequency normalized by the quarter-wavelength frequency (f_{bot}) for the depth at which each model joins the underlying halfspace. (c) The exponent η computed for the five velocity models that we consider the most realistic of the models used in this article, along with the average of η for the five models, the standard error of the mean, and the fit to the mean given by equations (8) and (9), with the coefficients in Table 2. The color version of this figure is available only in the electronic edition.

models considered in the article. We call these amplifications "A_{SRImod}" (or "SRImod" in the figures) even though this is a misnomer because "SRI" stands for "square-root impedance" (i.e., $\eta = 0.5$). More accurate acronyms might be "IPE" or "ZPE" (Impedance raised to the Power Eta), but for now we use A_{SRImod} to indicate that the amplifications are obtained by a modification of A_{SRI}, as given by $A_{\mathrm{SRImod}} = (A_{\mathrm{SRI}})^{\frac{\eta}{0.5}}$.

Comparisons of the amplifications and the FR/SRI ratios for all of the velocity models used in this article are given in Figures 11–13. $A_{\mathrm{FR}}/A_{\mathrm{SRImod}}$ for three of these models (all of which have $V_{S30} = 760$ m/s) are shown in Figure 11 (which

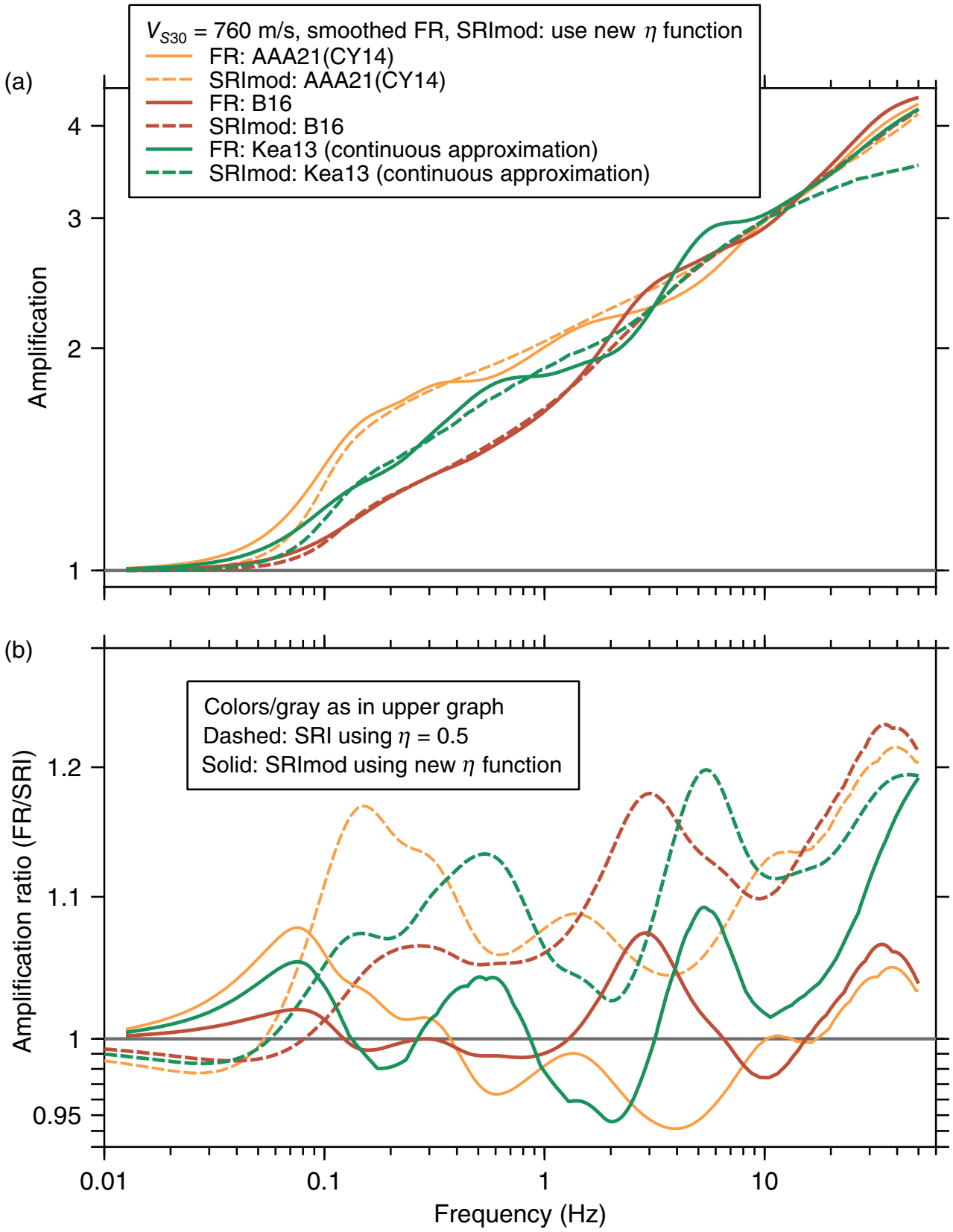

Figure 11. The equivalent of Figure 2 but with SRI amplifications replaced by SRImod amplifications (panel a). For comparison, panel (b) includes the ratios of the FR amplifications to the SRI (dashed) and SRImod (solid) amplifications. The color version of this figure is available only in the electronic edition.

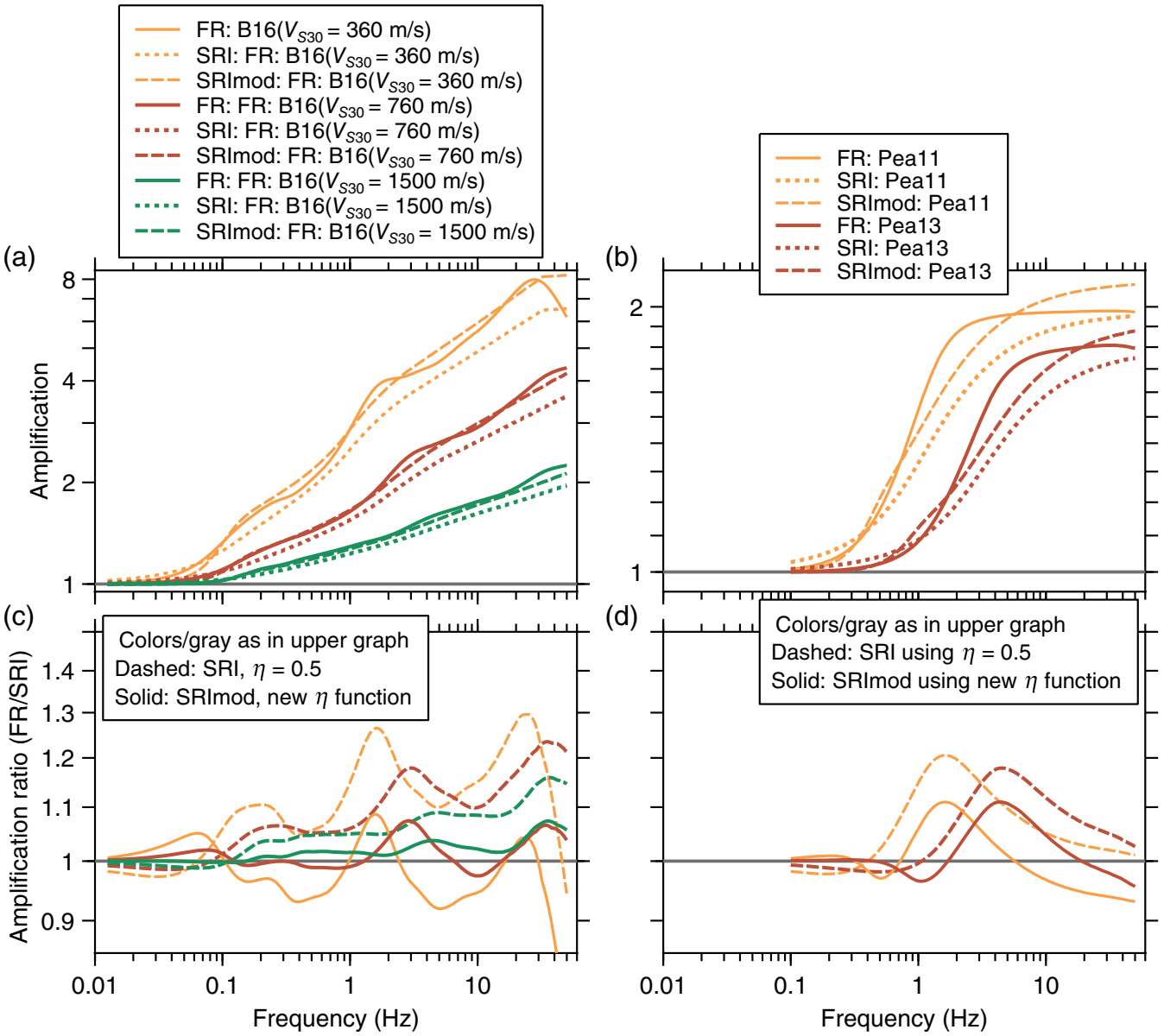

Figure 12. (a) Amplifications for three profiles with different values of V_{S30} (see legend for details). (b) Amplifications for the two Poggi *et al.* (2011, 2013) velocity profiles. (c,d) Ratios of the amplifications shown in panels (a) and (b), respectively. The FR, SRI, and SRImod amplifications and their ratios for five velocity models (the results for B16 [V_{S30} = 760 m/s] are the same as in Figure 11 but are included here because they are part of the Boore, 2016 [B16] set of models). The color version of this figure is available only in the electronic edition.

is the equivalent of Fig. 2). A_{SRImod} for the three velocity models is much closer to A_{FR} than A_{SRI}. The ratio of A_{FR} to A_{SRImod} is no longer predominately one sided, with A_{FR} being larger than A_{SRI}, and A_{SRImod} is generally within 5% of A_{FR}. The results for the other two models used in computing the mean η (B16, with V_{S30} = 360 and 1500 m/s) are shown in the graphs on the first column of Figure 12 (with the results for the B16, V_{S30} = 760 m/s model repeated from Fig. 11). Of course, the new η function was obtained such that on average, A_{SRImod} equals A_{FR} for the five velocity models used in the fitting. The graphs in the second column of Figure 12 show results for the Poggi *et al.* (2011, 2013) models; those models are very

TABLE 2
Coefficients of the Function in Equation (8)

Coefficient	Value
a	0.560
b	−1.301
s	1.398
d	4.000
e	6.000
g	2.000
h	0.760
p	3.000
q	0.333

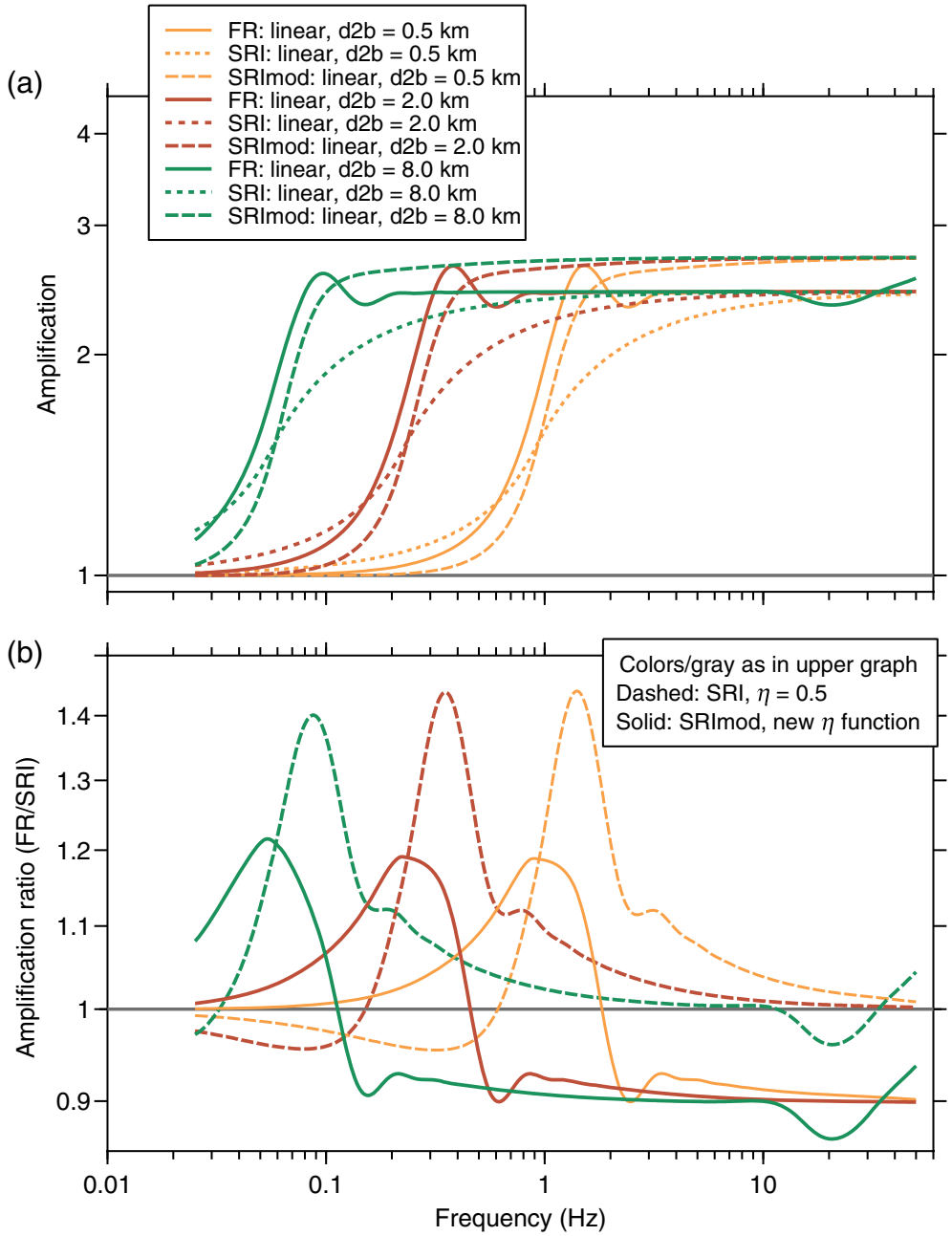

Figure 13. (a) The FR, SRI, and SRImod amplifications and (b) their ratios for three velocity models. The color version of this figure is available only in the electronic edition.

different than the other models considered in the article and were not used in deriving the η function, yet A_{SRImod} for these models is generally closer to A_{FR} than are the original A_{SRI}. For completeness, Figure 13 shows the comparisons for the models with linear dependence of velocity on depth. Even for these unrealistic models, the SRImod amplifications reduce the maximum amplitudes of the mismatch between A_{FR} and A_{SRI}. On balance, we think that the η function in equation (8), with the coefficients in Table 2, provides a useful modification to A_{SRI} by bringing them closer to A_{FR} via a simple, easy-to-implement revision of A_{SRI}. The improvement is not perfect, but it is model independent and should be useful for the types of models often used in computing crustal amplifications.

DISCUSSION AND CONCLUSIONS

The frequencies of the amplification peaks for the CVL profiles and the comparison of A_{FR} and A_{SRI} with those from the gradient profiles give some support to the hypothesis that the difference between A_{FR} and A_{SRI} for gradient profiles is because the former is controlled by the ratio of seismic impedances, but the latter is based on the square root of the seismic impedance ratios. This implies that gradient profiles will always have $A_{\mathrm{FR}} > A_{\mathrm{SRI}}$ (as is well known to be true for the peak amplitudes of the fundamental mode resonances for profiles with strong impedance contrasts between layers). The one exception is that A_{SRI} can be larger than A_{FR} for low frequencies corresponding to depths in the half-space below the velocity profile, but in this case, both A_{SRI} and A_{FR} are close to unity. The differences in A_{FR} and A_{SRI} for gradient profiles are not large, however, and even though A_{FR} is easy to compute, there are advantages to using the SRI method to compute amplifications. A number of these advantages are discussed in B13. These include the rapidity of computing site amplifications for a wide variety of velocity models without depending on the details of the velocity model, the association of a frequency of the amplification with each depth, and the smoothing over the many peaks and troughs usually seen in theoretical FR calculations. (These peaks and troughs are often not seen in average site-specific response calculated from real data, as shown by, e.g., Thompson *et al.*, 2009.) An advantage not included in B13 is that the equations for computing A_{SRI} allow for analytical

equations to be used in inferring velocity profiles from ground-motion prediction profiles (Al Atik and Abrahamson, 2021). A modification of A_{SRI} given using an exponent η different than the value of 0.5 used in the original definition of A_{SRI} is proposed in this article. This modification shows promise in bringing A_{SRI} closer to A_{FR}, increasing the usefulness of the simple and rapid amplifications given using impedance ratios involving QWL frequency-dependent averages of velocity over depth.

DATA AND RESOURCES

Aside from the velocity profiles, no data were used in this article. The velocity profiles were either constructed by us or were taken from the references cited in the figures and text. The amplifications used the following programs from the SiteAmp suite of Fortran programs: site_amp_batch, f4nrattle, nrattle, and vel2cvl_profile. The program site_amp_batch has been revised to include computations of A_{SRImod}, using η determined both from equation (8) and from interpolation of the mean η shown in Figure 10c (thus avoiding the mismatch between the function and the mean η at small values of f/f_{bot}). The SiteAmp suite of programs is part of the SMSIM suite of programs (Boore, 2005) available from http://www.daveboore.com/software_online.html. Unpublished notes in constructing constant-velocity layered profiles are at Constructing_equivalent_constant-velocity_layered_profiles.2021-10-26.pdf, available at https://www.daveboore.com/daves_notes.html. The figures were prepared using CoPlot available at https://www.cohortsoftware.com. All websites were last accessed in January 2023.

DECLARATION OF COMPETING INTERESTS

The authors acknowledge that there are no conflicts of interest recorded.

ACKNOWLEDGMENTS

The differences in full-resonance (FR) and square-root-impedance (SRI) amplifications for gradient profiles was brought to the first author's attention in a 2010 technical note by Frank Scherbaum sent to the first author by Philippe Renault in 2011. The first author thanks Linda Al Atik for again drawing his attention, in 2021, to the differences and for reminding him that he had discussed this in his 2013 article (Boore, 2013). The authors thank Annemarie Baltay, John Douglas, Geneva Chong, Roberto Paolucci, Grace Parker, Eric Thompson, and an anonymous reviewer for constructive comments and Yousef Bozorgnia for providing a reference. Any use of trade, firm, or product names is for descriptive purposes only and does not imply endorsement by the U.S. Government.

REFERENCES

Al Atik, L., and N. Abrahamson (2021). A methodology for the development of 1D reference V_S profiles compatible with ground-motion prediction equations: Application to NGA-West2 GMPEs, *Bull. Seismol. Soc. Am.* **111,** 1765–1783.

Al Atik, L., and R. R. Youngs (2014). Epistemic uncertainty for NGA-West2 models. *Earthq. Spectra* **30,** 1301–1318.

Boore, D. M. (2003). Prediction of ground motion using the stochastic method, *Pure Appl. Geophys.* **160,** 635–676.

Boore, D. M. (2005). SMSIM—Fortran programs for simulating ground motions from earthquakes: Version 2.3—A revision of OFR 96-80-A, *U. S. Geol. Surv. Open-File Rept. 00-509*, revised 15 August 2005, 55 pp.

Boore, D. M. (2013). The uses and limitations of the square-root impedance method for computing site amplification, *Bull. Seismol. Soc. Am.* **103,** 2356–2368.

Boore, D. M. (2016). Determining generic velocity and density profiles for crustal amplification calculations, with an update of the Boore and Joyner (1997) generic site amplification for $\bar{V}_S(z) = 760$ m/s, *Bull. Seismol. Soc. Am.* **106,** 316–320.

Boore, D. M., and W. B. Joyner (1997). Site amplifications for generic rock sites, *Bull. Seismol. Soc. Am.* **87,** 327–341.

Chiou, B. S. J., and R. R. Youngs (2014). Update of the Chiou and Youngs NGA profile for the average horizontal component of peak ground motion and response spectra, *Earthq. Spectra* **30,** 1117–1153.

Day, S.M. (1996). RMS response of a one-dimensional halfspace to *SH*, *Bull. Seismol. Soc. Am.* **96**, 363–370.

Douglas, J., P. Gehl, L. F. Bonilla, O. Scotti, J. Régnier, A.-M. Duval, and E. Bertrand (2009). Making the most of available site information for empirical ground-motion prediction, *Bull. Seismol. Soc. Am.* **99,** 1502–1520.

Kamai, R., N. Abrahamson, and W. Silva (2013). Nonlinear horizontal site response for the NGA-West2 project, *PEER Rept No. 2013/12*, Pacific Earthquake Engineering Research Center, University of California, Berkeley, Berkeley, California.

Poggi, V., B. Edwards, and D. Fäh (2011). Derivation of a reference shear-wave velocity profile from empirical site amplification, *Bull. Seismol. Soc. Am.* **101,** 258–274.

Poggi, V., B. Edwards, and D. Fäh (2013). Reference S-wave velocity profile and attenuation profiles for ground-motion prediction equations: Application to Japan, *Bull. Seismol. Soc. Am.* **103,** 2645–2656, doi: 10.1785/0120120362.

Schreyer, H. L. (1977). One-dimensional elastic waves in inhomogeneous media, *J. Eng. Mech. Div.* **103,** 979–990.

Thompson, E. M., L. G. Baise, R. E. Kayen, and B. B. Guzina (2009). Impediments to predicting site response: Seismic property estimation and modeling simplifications, *Bull. Seism. Soc. Am.* **99,** 2927–2949.

Manuscript received 6 October 2022
Published online 28 February 2023